Dan Yuan[1]
Sharda Yadav[2]
Hang T. Ta[2]
Hedieh Fallahi[2]
Hongjie An[2]
Navid Kashaninejad[2]
Chin Hong Ooi[2]
Nam-Trung Nguyen[2]
Jun Zhang[2]

[1]Centre for Regional and Rural Futures, Deakin University, Geelong, Victoria, 3216, Australia
[2]Queensland Micro- and Nanotechnology Centre, Griffith University, Nathan, Queensland, 4111, Australia (E-mail: nam-trung.nguyen@griffith.edu.au)

Received April 30, 2021
Revised July 26, 2021
Accepted August 5, 2021

Research Article

Investigation of viscoelastic focusing of particles and cells in a zigzag microchannel

Microfluidic particle focusing has been a vital prerequisite step in sample preparation for downstream particle separation, counting, detection, or analysis, and has attracted broad applications in biomedical and chemical areas. Besides all the active and passive focusing methods in Newtonian fluids, particle focusing in viscoelastic fluids has been attracting increasing interest because of its advantages induced by intrinsic fluid property. However, to achieve a well-defined focusing position, there is a need to extend channel lengths when focusing micrometer-sized or sub-microsized particles, which would result in the size increase of the microfluidic devices. This work investigated the sheathless viscoelastic focusing of particles and cells in a zigzag microfluidic channel. Benefit from the zigzag structure of the channel, the channel length and the footprint of the device can be reduced without sacrificing the focusing performance. In this work, the viscoelastic focusing, including the focusing of 10 μm polystyrene particles, 5 μm polystyrene particles, 5 μm magnetic particles, white blood cells (WBCs), red blood cells (RBCs), and cancer cells, were all demonstrated. Moreover, magnetophoretic separation of magnetic and nonmagnetic particles after viscoelastic pre-focusing was shown. This focusing technique has the potential to be used in a range of biomedical applications.

Keywords:
Magnetophoresis / Particle focusing / Particle separation / Viscoelastic fluid
DOI 10.1002/elps.202100126

Additional supporting information may be found online in the Supporting Information section at the end of the article.

1 Introduction

Microfluidic devices have the advantages of reduced sample volume needed, lower cost, relatively high efficiency, and accuracy [1–6]. Because of these advantages, they have been proven as promising platforms for the manipulation of both biological and synthetic particles in a broad range of fields including biology, chemistry and medical science [7–10]. Among all kinds of particle manipulation, microfluidic particle focusing always serves as a prerequisite step for downstream particle separation [11–13], counting [14], detection, or analysis [15–17]. Moreover, the ability to position particles in a tightly focused stream is essential for various flow cytometry [18], such as imaging flow cytometry [15,19,20], Raman flow cytometry [21], and deformability cytometry [22,23].

Particle focusing in a Newtonian fluid has been extensively studied using both active and passive methods [11,24–26]. Active methods are based on the external force fields, such as dielectrophoresis [27,28], magnetophoresis [29,30], acoustophoresis [31], and optical tweezers [32]. Passive methods rely on intrinsic hydrodynamic forces which are induced by specialized designed channel geometry or structures [33–35], such as pinched flow fractionation (PFF) [36], deterministic lateral displacement (DLD) [37], hydrodynamic filtration [38], and inertial microfluidics [24,39,40].

The microfluidic particle focusing methods mentioned above are all performed in Newtonian fluids, while particle manipulation methods utilizing viscoelastic fluids have been increasingly attracting interest from the research community. Particles suspended in a viscoelastic fluid would experience flow-induced elastic lift force, inertial lift force, and drag force. Particle trajectories and equilibrium positions are tuned by the competition of these forces. Based on the intrinsic elastic properties of viscoelastic fluids, the need for external force fields or complex channel geometries for efficient particle focusing can be eliminated [41–47]. The advantages of viscoelastic fluids allow the fast growth of

Correspondence: Dr. Jun Zhang, Queensland Micro- and Nanotechnology Centre, Griffith University, Nathan, Queensland 4111, Australia.
E-mail: jun.zhang@griffith.edu.au
Additional corresponding author: Professor Nam-Trung Nguyen
E-mail: nam-trung.nguyen@griffith.edu.au

Abbreviations: **PEO**, poly(ethylene oxide); **RBCs**, red blood cells; **WBCs**, white blood cells

Color online: See article online to view Figs. 1–6 in color.

microfluidic techniques and applications for particle focusing. The viscoelastic particle focusing has been investigated extensively in straight channels with cylindrical [48–50] and rectangular cross-sections [51–54], spiral microchannels [55–57], straight channels with sidewalls [12,58], and symmetric serpentine microchannels [59]. However, to achieve a well-defined focusing position, there is a need to extend channel length when focusing micrometer-sized or sub-microsized particles [59–61], which would result in the size increase of the microfluidic devices.

To address the above problem, this work investigated the sheathless focusing of particles and cells in viscoelastic fluids in a zigzag microfluidic channel and particle separation combined with positive magnetophoresis. Benefit from the zigzag structure, the channel length and the footprint of the device can be reduced without sacrificing the focusing performance. In this work, the viscoelastic focusing for a variety of particles and cells, including 10 μm polystyrene particles, 5 μm polystyrene particles, 5 μm magnetic particles, white blood cells (WBCs), red blood cells (RBCs), and cancer cells was evaluated. Moreover, magnetophoretic separation of magnetic and nonmagnetic particles after viscoelastic pre-focusing was performed as well. This focusing technique can serve as a pre-ordering unit in flow cytometry or other cell counting, sorting, and analysis systems.

2 Materials and methods

2.1 Design and fabrication of the microfluidic device

The microfluidic device consists of three zigzag periods for particle viscoelastic focusing and an expanded channel for magnetic deflection, as shown in Fig. 1A. The width of the zigzag microchannel is 50 μm. The lengths of long and short zigzag sides are 5 and 0.6 mm, respectively. At the end of the zigzag section, the width of the microchannel expands from 50 to 600 μm. A permanent neodymium magnet with a dimension of 4 × 5 × 10 mm (height × width × length) is located 1 mm away from the expanded channel. The height of all microchannels is uniform as 50 μm. The microfluidic device was fabricated by standard photolithography and PDMS soft lithography techniques [62,63]. The photo of the fabricated device was shown in Fig. 1C. The dimensions of the PDMS channel part are approximately 50 × 10 × 5 mm (length × width × height). The PDMS channel slab was bonded to a microscope glass slide (length × width = 76 × 25 mm).

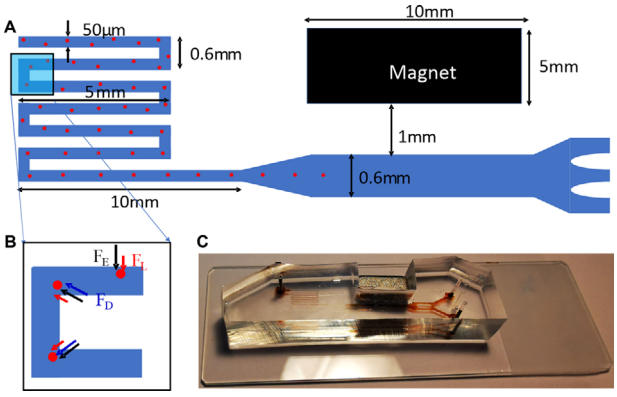

Figure 1. (A) Diagram of microchannel structure and dimension. (B) Particle migration at the U-turn of the zigzag channel. (C) The photo of fabricated microfluidic device.

2.2 Preparation of PEO solution and particles

For viscoelastic focusing, poly(ethylene oxide) (PEO, Mw = 600 000 Da, Sigma-Aldrich) was dissolved in PBS (Thermo Fisher Scientific, Product No.10010023) with a concentration of 1000 ppm to form the viscoelastic fluid. As referenced in the previous work [64], the properties of prepared PEO solutions are listed in Supporting Information Table 1. The effective relaxation times of prepared PEO solutions λ were estimated from previous ones measured with capillary breakup extension rheometry (CaBER) [65]. λ can be defined as $\lambda = 18\lambda_z(c/c^*)^{0.65}$, where c is polymer concentration, and $c^* = 0.77/[\eta]$ is the polymer overlap concentration (the intrinsic viscosity $[\eta] = 0.072M_W{}^{0.65}$) [66]. $\lambda_z = f[\eta](M_w)\eta_s/RT$ is the relaxation time predicted by Zimm theory [66,67], where f (= 0.463) is the prefactor dependent upon the solvent quality, η_s (= 1 × 10^{-3} Pa·s) is the solvent viscosity, R (= 8.314 J/mol•K) is the gas constant, and T (= 293 K) is the absolute temperature. The dynamic viscosity $\mu_f = \eta_s + \eta_p = \eta_s + 0.072c\eta_s M_W{}^{0.65}$, η_p is the polymeric contribution to the solution viscosity and can be expressed as $[\eta]c\eta_s = 0.072c\eta_s M_W{}^{0.65}$.

Nonmagnetic polystyrene microbeads with diameters of 5 μm (Thermo Fisher Scientific, Product No. G0500, CV5%), and 10 μm (Thermo Fisher Scientific, Product No. G1000, CV5%) and magnetic particles (Sigma-Aldrich, Product No. 39 689) were respectively dispersed in the 1000 ppm PEO solution at a concentration from 10^5 to 10^6 counts/mL. Tween 20 (Sigma-Aldrich, Product No. P9416) with 0.1% w/v was added to prevent particles from aggregation.

2.3 Preparation of blood cells

Human whole blood was provided by the Australian Red Cross Lifeblood (Brisbane, Australia) under the Material Supply Deed number 20-02QLD-11. The ethics approval was obtained from Griffith University/University of Queensland (Approval number: 2020/233 and 2 015 001 037). WBCs were isolated based on the protocol provided by the company by centrifugation using a density gradient medium (Leuko Spin Medium, pluriSelect Life Science UG and Co. KG). In brief, the double volume of PBS was added to the blood sample for dilution. Then, the blood sample was carefully layered on top of the density gradient medium and centrifuged at 1000 × *g* for 30 min. Subsequently, the WBCs fraction was removed

from the medium and washed twice. The RBCs were collected from the bottom of the centrifuge tube and washed twice using PBS. Finally, WBCs and RBCs were suspended in the prepared viscoelastic PEO solution.

2.4 Experimental setup

An inverted microscope (Nikon, Eclipse TS100) was used for observation of the microfluidic device. Particle and cell suspensions were infused into the microfluidic device at specific flow rates by a syringe pump (Cetoni GmbH, neMESYS 290N). A high-speed CCD camera (Photron, FASTCAM SA3) was mounted on the microscope and captured the movement videos of single particles at an ultra-short (~20 μs) exposure time. The open-source software ImageJ (National Institutes of Health USA) was used to analyze the captured videos. The single-particle images were stacked so that the statistical distribution of particles per cells can be visualized.

3 Theory

3.1 Inertial lift force

In a Newtonian fluid, the particle migration is governed by inertial lift force F_L. The inertial lift force is the sum of two lift forces: shear gradient lift force (F_{LS}) and wall-repulsion force (F_{LW}). The inertial lift forcecan be expressed as [39,68]:

$$F_L = \frac{\rho_f U_m^2 a^4}{D_h^2} f_L\,(\mathrm{Rc}, x_c) \tag{1}$$

$$\mathrm{Rc} = \frac{\rho_f U_m D_h}{\mu_f} = \frac{2\rho_f Q}{\mu_f\,(w+h)} \tag{2}$$

where ρ_f, U_m, and μ_f are the fluid density, mean velocity, and dynamic viscosity, respectively; a is the spherical diameter of the particles; $D_h = 2wh/(w+h)$ is the hydraulic diameter for a rectangular channel with w and h the width and height of the channel cross-section. Q is the volumetric flow rate. The lift coefficient of the net inertial lift force $f_L(\mathrm{Rc}, x_c)$ is a function of the position of the particles within the cross-section of the channel x_c and the channel Reynolds number Rc [39].

3.2 Elastic force

In a viscoelastic fluid, an additional elastic force induced by polymer is applied on particles. The elastic effects of the viscoelastic fluids are characterized by Weissenberg number *Wi* [52]:

$$Wi = \frac{\lambda}{t_f} = \lambda\dot{\gamma} = \lambda\frac{2U_m}{w} = \frac{2\lambda Q}{hw^2} \tag{3}$$

where λ is the relaxation time of the fluid, t_f is the characteristic time of the channel flow. The characteristic time is approximately equal to the inverse of the average (characteristic) shear rate $\dot{\gamma}$, which is $2U_m/w$ or $2\lambda Q/hw^2$in a rectangular channel with w and h the width and height of the channel cross-section.

Elasticity number, *El*, is defined as the ratio of Weissenberg number *Wi* to Reynolds number Rc

$$El = \frac{Wi}{Rc} = \frac{\lambda\mu_f\,(w+h)}{\rho_f w^2 h} \tag{4}$$

In viscoelastic fluids, both the first normal stress N_1 ($= \tau_{xx} - \tau_{yy}$) and the second normal stress N_2 ($= \tau_{yy} - \tau_{zz}$) contribute to particle migration. τ_{xx}, τ_{yy}, and τ_{zz} are normal stresses exerted along the main flow, the velocity gradient, and vorticity direction, respectively. However, the effects of N_2 can be neglected in diluted polyethylene oxide (PEO) solutions [69,70], because N_1 is much larger than N_2. The elastic force F_E, which originates from an imbalance in the distribution of N_1 over the size of the particle, can be expressed as [43]:

$$\begin{aligned} F_E &= C_{eL} a^3 \nabla N_1 = C_{eL} a^3 \left(\nabla\tau_{xx} - \nabla\tau_{yy}\right) \\ &= -2C_{eL} a^3 \eta_p \lambda \nabla\dot{\gamma}^2 \end{aligned} \tag{5}$$

where C_{eL} is the nondimensional elastic lift coefficient. η_p is the polymeric contribution to the solution viscosity.

3.3 Drag force

A drag force arises when an object moves through a fluid or when the fluid flows past an object, due to a velocity difference between particle and fluid, and it is expressed as [24,39]

$$F_D = 3\pi\mu_f a\left(v_f - v_p\right) \tag{6}$$

where v_f and v_p are the velocities of the fluid element and particles, respectively.

3.4 Magnetophoretic force

Magnetophoretic force can alter the motion of a magnetic particle in a viscous medium under the influence of an external magnetic field, which can be expressed as [71]:

$$F_{mag} = \mu_0 V_p \left[\left(M_p - M_f\right) * \nabla\right] H \tag{7}$$

where μ_0 is the permeability of free space ($4\pi \times 10^{-7}$ $\mathrm{H/m^{-1}}$), V_p is the volume of the particle, M_p is the magnetization of the magnetized particle, M_f is the magnetization of the fluid, and H is the magnetic field at the center of the particle. The dimensionless group *Rc*, *Wi*, and *El* under different flow rates have been calculated and summarized in Supporting Information Table 2.

4 Results and discussion

4.1 Particle migration in zigzag channel

When particles flow in a zigzag channel in viscoelastic fluids, the particles would experience three different kinds of forces: inertial lift force F_L, which consists of the shear-gradient lift force (F_{LS}) and wall-repulsion force (F_{LW}); elastic force F_E, resulting from the nature of the viscoelastic medium, and the Dean drag force F_D, induced by the bent structure at each turning point. When particles flow in a straight channel instead of a zigzag channel in viscoelastic fluids, the particles will experience inertial and elastic forces, Fig. 1B. The shear gradient lift force pushes particles away from the centerline of the channel, while the wall lift force drives particles away from the channel wall. At the same time, the viscoelastic force directs away from the wall and declining with increasing distance from the wall. Moreover, because of the zigzag structure of the channel, at each turning point, the Dean drag force acts in superposition on the particles, which is perpendicular to the main flow direction, directing from the inner corner to the outer corner. The particles can be focused under the synergetic effect of inertial lift force F_L, the Dean drag force F_D, and elastic force F_E. The zigzag channel is bending alternatively so that the direction of Dean drag force is varied periodically. The net effect is that the Dean drag force will promote the focusing at the channel center. After a given distance, these particles can be focused within a certain width at the center of the channel.

4.2 Viscoelastic focusing of nonmagnetic and magnetic particles

We characterized the viscoelastic focusing performance of the proposed zigzag channel using both nonmagnetic particles and magnetic particles. 10 μm polystyrene beads were suspended in the 1000 ppm PEO solution and infused into the microchannel at flow rates from 2 to 24 μL/min. Figure 2A shows the particle distribution after each zigzag period at the flow rate of 10 μL/min. We can see that particles spread widely near the channel center after first zigzag period (Fig. 2A). The distribution region shrinks gradually after the consecutive zigzag periods and finally forms a single particle train at the channel center.

Furthermore, we can see that focusing performance is optimal at a moderate flow rate from 8 to 20 μL/min. Within this flow region, particles can focus narrowly and the width of the focusing band can even be as small as one particle diameter (Fig. 2B). The lateral distribution of particles along the channel width can be amplified at the expansion region (Fig. 2C). When the flow rate is below 8 μL/min, the elastic force is insufficient to push particles into the channel center. Moreover, when the flow rate exceeds 20 μL/min, more particles escape the focusing area with an increasing flow rate, which may be due to the rising inertial effects.

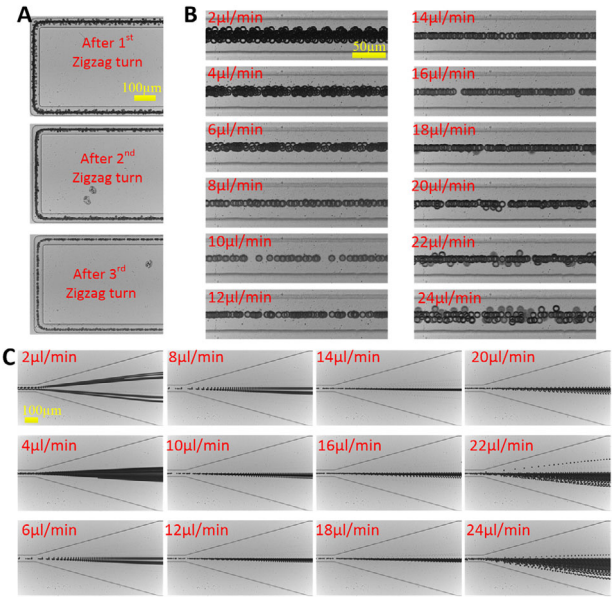

Figure 2. Viscoelastic focusing of 10 μm polystyrene particles in the proposed zigzag channel. (A) Particle distribution at different locations. (B) Particle distribution under various flow rates. (C) Particle distribution at the expansion area.

Besides, we characterized the focusing properties of 5 μm polystyrene beads in the proposed channel. Similar to that of 10 μm particles, the focusing band of 5 μm particles reduces gradually after passing through the subsequent zigzag periods (Fig. 3A). However, the width of the optimal focusing band is about two times of particle diameter. This focusing performance is worse than the 10 μm particles, for which the focusing band can be as small as one particle diameter. Furthermore, below 8 μL/min, the focusing quality of 5 μm particles is relatively poor (Fig. 3B and C). Surprisingly, we found that the optimal focusing performance can maintain at flow rates from ∼8 to ∼32 μL/min, much broader than that of 10 μm particles. This indicates that the proposed device can tolerate a wide flow range for the optimal focusing of small particles.

After that, we characterized the viscoelastic focusing of 5 μm magnetic particles, which is composited by polystyrene and iron oxide. The density of magnetic particles is 1530 kg/m^3, much denser than the suspended medium (∼1000 kg/m^3). Therefore, in the vertical direction, the particle gravity will affect the balance position of particles. We can see that the most magnetic particles can be focused decently along the channel center (Fig. 4). However, a few of them escape and deflect slightly from the focusing band, making the focusing properties worse than nonmagnetic polystyrene particles.

4.3 Viscoelastic focusing of blood cells

After the characterization of polystyrene beads, we further evaluated the focusing performance of the zigzag channel on

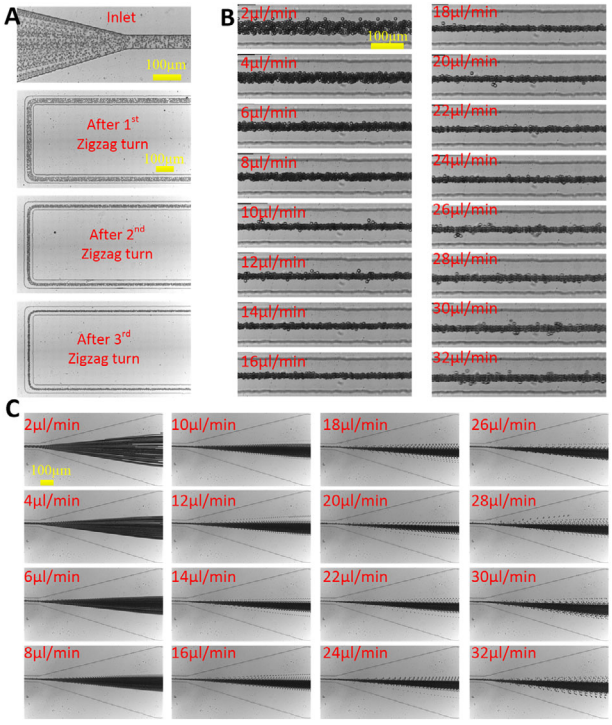

Figure 3. Viscoelastic focusing of 5 μm polystyrene particles in the zigzag channel. (A) Particle distribution at different locations. (B) Particle distribution under various flow rates. (C) Particle distribution at the expansion area.

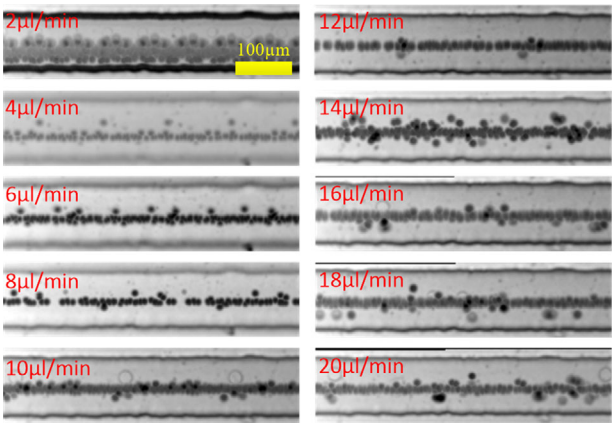

Figure 4. Viscoelastic focusing of 5 μm magnetic particles in the zigzag channel under different flow rates.

blood cells (i.e., RBCs and WBCs), Fig. 5. The WBCs were isolated using density gradient centrifugation and then suspended in the PEO solution. The infusion flow rate was from 2 to 24 μL/min. From Fig. 5A and B, we observed that WBCs have a similar focusing trend as 10 μm polystyrene beads, but the focusing performance is not as good as polystyrene beads. A total of 10 μm polystyrene beads can focus as a single particle train at the channel center. In contrast, the WBCs clearly show deflection from the channel center. The relatively poor focusing performance is probably due to the nonspherical shape of WBCs, a wide size range (8–16 μm) [72], and cell deformability.

We also characterized the focusing properties of RBCs in the proposed device. RBCs are discoid, with ~8 μm in diameter and ~2.5 μm in thickness. The focusing properties of RBCs are close to that of 5 μm polystyrene beads. When the flow rate is over 10 μL/min, the RBCs can maintain a fair focusing status, and the focusing streak width is around three times of cell diameter, (Fig. 5C and D). Besides, we also evaluated the viscoelastic focusing performance of cancer cells in the proposed channel, as shown in Supporting Information Fig. 1.

4.4 Magnetic separation of particles

Magnetophoretic force can alter the motion of a magnetic particle in a viscous medium under the influence of an external magnetic field. For most nonmagnetic natural bioparticles such as cells, the functionalized magnetic beads can attach to the bioparticles. In this way, a magnetic property can be endowed to bioparticles. Many previous works utilized sheath flow to pinch sample flow and confine to one sidewall at the inlet [73,74], and magnetic particles can be attracted and detached from their nonmagnetic counterparts. However, the utilization of sheath flow has the disadvantages of diluting the original sample and requiring more external components, which complicate the flow control and the overall system. In this work, we utilized the three-dimensional focusing function of the viscoelastic fluid, avoiding sheath flow. Modifying the reported works using straight channels [75–77] as a pre-focusing unit, we developed the zigzag channel, which consisted of bent straight channel sections. The advantage of the zigzag channel is that it can significantly reduce the device footprint, especially for small particles, a lengthy channel is always needed, making the device footprint unnecessarily large and constraining the design of other functional units. Thus, a zigzag channel can multiply the overall length by connecting many parallel channels. Besides, the secondary flow induced at the zigzag U-turn can also promote viscoelastic focusing [59].

In this work, the elastic pre-focusing in the zigzag channel was combined with the magnetic deflection to demonstrate the sheathless separation. The mixture of 5 μm nonmagnetic polystyrene beads and magnetic beads were dispersed in the 1000 ppm PEO solution. The mixture was infused into the designed device at a flow rate of 10 μL/min. A permanent magnet is placed downstream with a lateral distance of 1 mm. From Fig. 6, we can see that both magnetic and nonmagnetic particles are focused narrowly at the end of the zigzag channel, and they enter the expanded channel section, Fig. 6A(i) and 6B(i). An external magnetic field in the expanded channel can exert a positive magnetophoretic force on magnetic particles. The expanded channel slows down the fluid flow velocity, so that the induced magnetic force can have sufficient time to alter the motion of particles, Fig. 6B(ii).

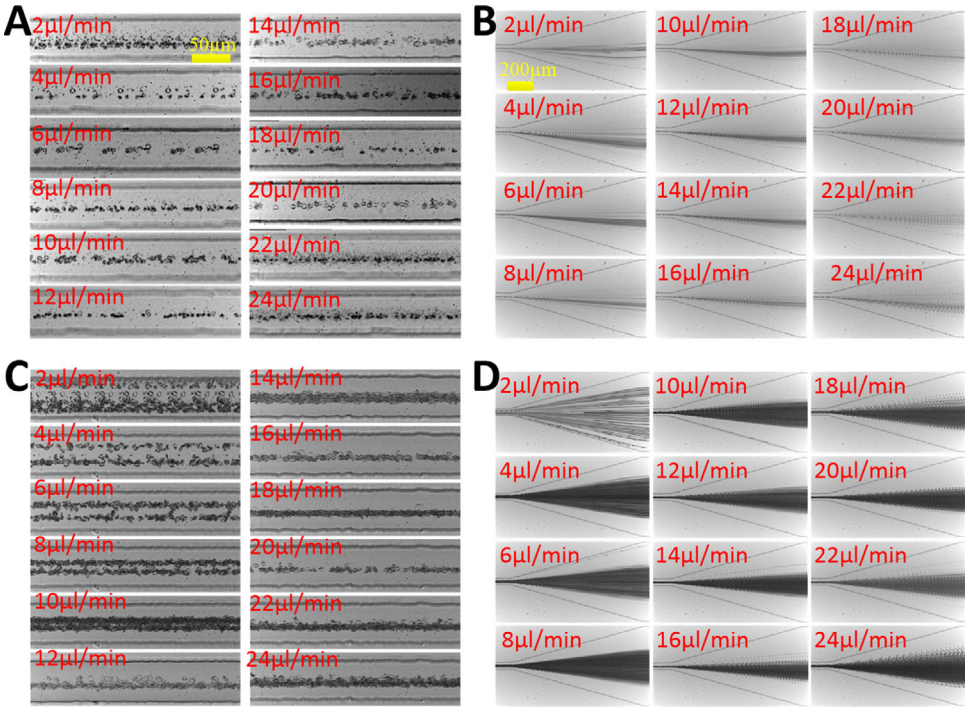

Figure 5. Viscoelastic focusing of white blood cells (WBCs) in the zigzag channel. (A) The distribution of WBCs at the end of zigzag channel. (B) WBCs distribution at the expansion region. (C) The distribution of red blood cells (RBCs) at the end of the zigzag channel. (D) RBCs distribution at the expansion region.

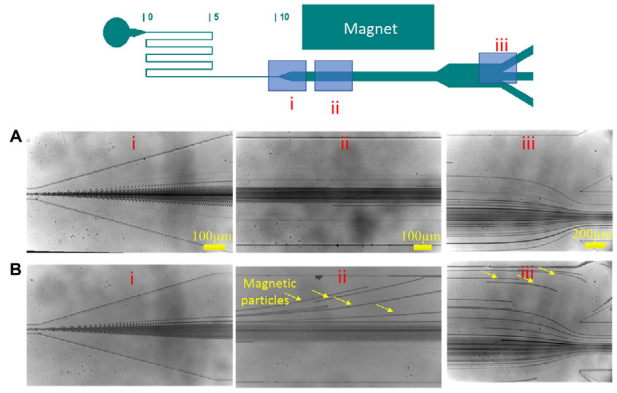

Figure 6. Magnetophoretic separation of magnetic and nonmagnetic particles after viscoelastic pre-focusing. (A) Magnetic and nonmagnetic particles trajectories without magnetic field. (B) Magnetic and nonmagnetic particles trajectories under a magnetic field.

The magnetic particles were attracted to the magnet side and exited from the upper outlet, Fig. 6B(iii).

5 Concluding remarks

In this work, we investigated the sheathless viscoelastic focusing of particles and cells in a zigzag microchannel. The zigzag channel can multiply the overall length by connecting many parallel straight channel sections. Besides, the secondary flow induced at the U-turn can also promote viscoelastic focusing. We characterized the viscoelastic focusing properties of the zigzag channel using a variety of particles and cells, such as 10 µm polystyrene particles, 5 µm polystyrene particles, 5 µm magnetic particles, WBCs, RBCs, and cancer cells. Furthermore, magnetophoretic separation of magnetic and nonmagnetic 5 µm particles after viscoelastic pre-focusing was demonstrated. This focusing technique can be used in a range of biomedical applications, including cell separation, counting, detection and analysis.

Authors acknowledge the support from the Australian Research Council (ARC) Discovery Project (Grant No. DP180100055), ARC DECRA fellowship (Grant No. DE210100692) and Alfred Deakin Postdoctoral Research Fellowship.

The authors have declared no conflict of interest.

Data availability statement

The data in this study are available from the corresponding author upon reasonable request.

6 References

[1] Sackmann, E. K., Fulton, A. L., Beebe, D. J., *Nature* 2014, *507*, 181–189.

[2] Mark, D., Haeberle, S., Roth, G., Von Stetten, F., Zengerle, R., in: Kakaç, S., Kosoy, B., Li, D., Pramuanjaroenkij, A. (Eds.), *Microfluidics Based Microsystems: Fundamentals and Applications*, Springer, Dordrecht 2010, pp. 305–376.

[3] Song, C., Nguyen, N.-T., Tan, S.-H., Asundi, A. K., *Lab Chip* 2009, *9*, 1178–1184.

[4] Bandara, T., Nguyen, N.-T., Rosengarten, G., *Chem. Eng. Sci.* 2015, *126*, 283–295.

[5] Jiao, Z., Huang, X., Nguyen, N.-T., Abgrall, P., *Microfluid. Nanofluid.* 2008, *5*, 205–214.

[6] Nguyen, N.-T., Schubert, S., Richter, S., Dötzel, W., *Sens. Actuators, A* 1998, *69*, 85–91.

[7] Ota, N., Owa, Y., Kawai, T., Tanaka, Y., *J. Chromatogr. A* 2016, *1455*, 172–177.

[8] Gañán-Calvo, A., Montanero, J., Martín-Banderas, L., Flores-Mosquera, M., *Adv. Drug Delivery Rev.* 2013, *65*, 1447–1469.

[9] Jung, W., Han, J., Choi, J.-W., Ahn, C. H., *Microelectron. Eng.* 2015, *132*, 46–57.

[10] Shen, Y., Yalikun, Y., Tanaka, Y., *Sens. Actuators, B* 2019, *282*, 268–281.

[11] Whitesides, G. M., *Nature* 2006, *442*, 368–373.

[12] Yuan, D., Zhang, J., Yan, S., Pan, C., Alici, G., Nguyen, N.-T., Li, W., *Biomicrofluidics* 2015, *9*, 044108.

[13] Yuan, D., Tan, S. H., Zhao, Q., Yan, S., Sluyter, R., Nguyen, N.-T., Zhang, J., Li, W., *RSC Adv.* 2017, *7*, 3461–3469.

[14] Bhagat, A. A. S., Kuntaegowdanahalli, S. S., Kaval, N., Seliskar, C. J., Papautsky, I., *Biomed. Microdevices* 2010, *12*, 187–195.

[15] Nitta, N., Sugimura, T., Isozaki, A., Mikami, H., Hiraki, K., Sakuma, S., Iino, T., Arai, F., Endo, T., Fujiwaki, Y., *Cell* 2018, *175*, 266–276. e213.

[16] Yuan, D., Zhang, J., Sluyter, R., Zhao, Q., Yan, S., Alici, G., Li, W., *Lab Chip* 2016, *16*, 3919–3928.

[17] Nam, J., Shin, Y., Tan, J. K. S., Lim, B. Y., Lim, C. T., Kim, S., *Lab Chip* 2016, *16*, 2086–2092.

[18] Yan, S., Yuan, D., *Talanta* 2020, *221*, 121401.

[19] Isozaki, A., Mikami, H., Tezuka, H., Matsumura, H., Huang, K., Akamine, M., Hiramatsu, K., Iino, T., Ito, T., Karakawa, H., *Lab Chip* 2020, *20*, 2263–2273.

[20] Lei, C., Kobayashi, H., Wu, Y., Li, M., Isozaki, A., Yasumoto, A., Mikami, H., Ito, T., Nitta, N., Sugimura, T., *Nat. Protoc.* 2018, *13*, 1603–1631.

[21] Nitta, N., Iino, T., Isozaki, A., Yamagishi, M., Kitahama, Y., Sakuma, S., Suzuki, Y., Tezuka, H., Oikawa, M., Arai, F., *Nat. Commun.* 2020, *11*, 3452.

[22] Gossett, D. R., Henry, T., Lee, S. A., Ying, Y., Lindgren, A. G., Yang, O. O., Rao, J., Clark, A. T., Di Carlo, D., *Proc. Natl. Acad. Sci. USA* 2012, *109*, 7630–7635.

[23] Henry, T., Gossett, D. R., Moon, Y. S., Masaeli, M., Sohsman, M., Ying, Y., Mislick, K., Adams, R. P., Rao, J., Di Carlo, D., *Sci. Transl. Med.* 2013, *5*, 212ra163.

[24] Zhang, J., Yan, S., Yuan, D., Alici, G., Nguyen, N.-T., Warkiani, M. E., Li, W., *Lab Chip* 2016, *16*, 10–34.

[25] Khoo, B. L., Grenci, G., Lim, Y. B., Lee, S. C., Han, J., Lim, C. T., *Nat. Protoc.* 2018, *13*, 34.

[26] Vaidyanathan, R., Yeo, T., Lim, C. T., *Methods Cell Biol.* 2018, *147*, 151–173.

[27] Kang, Y., Li, D., Kalams, S. A., Eid, J. E., *Biomed. Microdevices* 2008, *10*, 243–249.

[28] Yan, S., Zhang, J., Alici, G., Du, H., Zhu, Y., Li, W., *Lab Chip* 2014, *14*, 2993–3003.

[29] Hejazian, M., Li, W., Nguyen, N.-T., *Lab Chip* 2015, *15*, 959–970.

[30] Zeng, J., Chen, C., Vedantam, P., Brown, V., Tzeng, T.-R. J., Xuan, X., *J. Micromech. Microeng.* 2012, *22*, 105018.

[31] Heyman, J. S., U.S. Patent 5 192 450, 1993.

[32] MacDonald, M., Spalding, G., Dholakia, K., *Nature* 2003, *426*, 421–424.

[33] Augustsson, P., Åberg, L. B., Swärd-Nilsson, A.-M. K., Laurell, T., *Microchim. Acta* 2009, *164*, 269–277.

[34] Yang, S., Ündar, A., Zahn, J. D., *Lab Chip* 2007, *7*, 588–595.

[35] Morton, K. J., Loutherback, K., Inglis, D. W., Tsui, O. K., Sturm, J. C., Chou, S. Y., Austin, R. H., *Lab Chip* 2008, *8*, 1448–1453.

[36] Yamada, M., Nakashima, M., Seki, M., *Anal. Chem.* 2004, *76*, 5465–5471.

[37] Davis, J. A., Inglis, D. W., Morton, K. J., Lawrence, D. A., Huang, L. R., Chou, S. Y., Sturm, J. C., Austin, R. H., *Proc. Natl. Acad. Sci. USA* 2006, *103*, 14779–14784.

[38] Crowley, T. A., Pizziconi, V., *Lab Chip* 2005, *5*, 922–929.

[39] Di Carlo, D., *Lab Chip* 2009, *9*, 3038–3046.

[40] Kuntaegowdanahalli, S. S., Bhagat, A. A. S., Kumar, G., Papautsky, I., *Lab Chip* 2009, *9*, 2973–2980.

[41] Yuan, D., Zhao, Q., Yan, S., Tang, S.-Y., Alici, G., Zhang, J., Li, W., *Lab Chip* 2018, *18*, 551–567.

[42] D'Avino, G., Greco, F., Maffettone, P. L., *Annu. Rev. Fluid Mech.* 2017, *49*, 341–360.

[43] Lu, X., Liu, C., Hu, G., Xuan, X., *J. Colloid Interface Sci.* 2017, *500*, 182–201.

[44] Faridi, M. A., Ramachandraiah, H., Banerjee, I., Ardabili, S., Zelenin, S., Russom, A., *J. Nanobiotechnol.* 2017, *15*, 1–9.

[45] Yuan, D., Zhang, J., Yan, S., Peng, G., Zhao, Q., Alici, G., Du, H., Li, W., *Electrophoresis* 2016, *37*, 2147–2155.

[46] D'Avino, G., Maffettone, P., *J. Non-Newtonian Fluid Mech.* 2015, *215*, 80–104.

[47] Yuan, D., Tan, S. H., Sluyter, R., Zhao, Q., Yan, S., Nguyen, N.-T., Guo, J., Zhang, J., Li, W., *Anal. Chem.* 2017, *89*, 9574–9582.

[48] D'Avino, G., Romeo, G., Villone, M. M., Greco, F., Netti, P. A., Maffettone, P. L., *Lab Chip* 2012, *12*, 1638–1645.

[49] Kang, K., Lee, S. S., Hyun, K., Lee, S. J., Kim, J. M., *Nat. Commun.* 2013, *4*, 2567.

[50] Seo, K. W., Byeon, H. J., Huh, H. K., Lee, S. J., *RSC Adv.* 2014, *4*, 3512–3520.

[51] Leshansky, A., Bransky, A., Korin, N., Dinnar, U., *Phys. Rev. Lett.* 2007, *98*, 234501.

[52] Yang, S., Kim, J. Y., Lee, S. J., Lee, S. S., Kim, J. M., *Lab Chip* 2011, *11*, 266–273.

[53] Xiang, N., Dai, Q., Ni, Z., *Appl. Phys. Lett.* 2016, *109*, 134101.

[54] Liu, C., Guo, J., Tian, F., Yang, N., Yan, F., Ding, Y., Wei, J., Hu, G., Nie, G., Sun, J., *ACS Nano* 2017, *11*, 6968–6976.

[55] Lee, D. J., Brenner, H., Youn, J. R., Song, Y. S., *Sci. Rep.* 2013, *3*, 3258.

[56] Liu, C., Ding, B., Xue, C., Tian, Y., Hu, G., Sun, J., *Anal. Chem.* 2016, *88*, 12547–12553.

[57] Xiang, N., Zhang, X., Dai, Q., Chen, J., Chen, K., Ni, Z., *Lab Chip* 2016, *16*, 2626–2635.

[58] Cha, S., Kang, K., You, J. B., Im, S. G., Kim, Y., Kim, J. M., *Rheol. Acta* 2014, *53*, 927–933.

[59] Yuan, D., Sluyter, R., Zhao, Q., Tang, S., Yan, S., Yun, G., Li, M., Zhang, J., Li, W., *Microfluid. Nanofluid.* 2019, *23*, 41.

[60] Brunn, P., *J. Non-Newtonian Fluid Mech.* 1980, *7*, 271–288.

[61] Asghari, M., Cao, X., Mateescu, B., Van Leeuwen, D., Aslan, M. K., Stavrakis, S., deMello, A. J., *ACS Nano* 2019, *14*, 422–433.

[62] Whitesides, G. M., Ostuni, E., Takayama, S., Jiang, X., Ingber, D. E., *Annu. Rev. Biomed. Eng.* 2001, *3*, 335–373.

[63] Nguyen, N.-T., Wereley, S. T., Shaegh, S. A. M., *Fundamentals and Applications of Microfluidics*, Artech House, Boston 2019.

[64] Liu, P., Liu, H., Yuan, D., Jang, D., Yan, S., Li, M., *Anal. Chem.* 2021, *93*, 1586–1595.

[65] Tirtaatmadja, V., McKinley, G. H., Cooper-White, J. J., *Phys. Fluids* 2006, *18*, 043101.

[66] Rodd, L. E., Scott, T. P., Boger, D. V., Cooper-White, J. J., McKinley, G. H., *J. Non-Newtonian Fluid Mech.* 2005, *129*, 1–22.

[67] Rodd, L. E., Cooper-White, J. J., Boger, D. V., McKinley, G. H., *J. Non-Newtonian Fluid Mech.* 2007, *143*, 170–191.

[68] Asmolov, E. S., *J. Fluid Mech.* 1999, *381*, 63–87.

[69] Magda, J., Lou, J., Baek, S., DeVries, K., *Polymer* 1991, *32*, 2000–2009.

[70] Pathak, J. A., Ross, D., Migler, K. B., *Phys. Fluids* 2004, *16*, 4028–4034.

[71] Zhu, T., Cheng, R., Liu, Y., He, J., Mao, L., *Microfluid. Nanofluid.* 2014, *17*, 973–982.

[72] Fallahi, H., Yadav, S., Phan, H.-P., Ta, H., Zhang, J., Nguyen, N.-T., *Lab Chip* 2021, *21*, 2008–2018.

[73] Vojtíšek, M., Tarn, M. D., Hirota, N., Pamme, N., *Microfluid. Nanofluid.* 2012, *13*, 625–635.

[74] Ngamsom, B., Esfahani, M. M., Phurimsak, C., Lopez-Martinez, M. J., Raymond, J.-C., Broyer, P., Patel, P., Pamme, N., *Anal. Chim. Acta* 2016, *918*, 69–76.

[75] Kim, M. J., Lee, D. J., Youn, J. R., Song, Y. S., *RSC Adv.* 2016, *6*, 32090–32097.

[76] Del Giudice, F., Madadi, H., Villone, M. M., D'Avino, G., Cusano, A. M., Vecchione, R., Ventre, M., Maffettone, P. L., Netti, P. A., *Lab Chip* 2015, *15*, 1912–1922.

[77] Zhang, J., Yan, S., Yuan, D., Zhao, Q., Tan, S. H., Nguyen, N.-T., Li, W., *Lab Chip* 2016, *16*, 3947–3956.

